Int. J. Electrochem. Sci., 7 **(2012)** 516 - 524

International Journal of
ELECTROCHEMICAL
SCIENCE
www.electrochemsci.org

Influence of 1-D Nano Rod Structure β-MnO_2 on Electrochemical Properties of Lithium Iron Phosphate

Xia Zheng[1,2], *Yongming Zhu* [1,*], *Peng Gao*[1], *Ning Li*[2], *Werner Weppner*[3]

[1] Department of Applied Chemistry, Harbin Institute of Technology at Weihai, Weihai 264200, China
[2] School of Chemical Engineering & Technology, Harbin Institute of Technology, Harbin 150001, China
[3] Faculty of Engineering, Institute of Materials Science, Christian-Albrechts-University, 24143 Kiel, Germany
[*]E-mail: hitonline@163.com

Received: 18 November 2011 / *Accepted:* 9 December 2011 / *Published:* 1 January 2012

Nano structure β-MnO_2 is successfully prepared via hydrothermal method, and dopes with $LiFePO_4$/C composite compounds. The presence of the β-MnO_2 doping is ascertained with the pine needle liked nano rods mixed with $LiFePO_4$/C particles by scanning electron microscopy (SEM). The doped β-MnO_2 does not affect the crystal structure of the $LiFePO_4$ core, as determined by X-ray diffraction (XRD). The β-MnO_2 doping can remarkably improve the interfacial resistance and the electrochemical performance of the cell. The β-MnO_2 doping $LiFePO_4$/C has a high discharge capacity of 165 mAh g^{-1} at C/10. This improvement may be due to the amelioration of the electrochemical dynamics on the $LiFePO_4$ electrode/electrolyte interface resulting from the effects of the 1-D nano rod structure β-MnO_2.

Keywords: 1-D Nano Rod; β-MnO_2; $LiFePO_4$/C; Hydrothermal Synthesis; Lithium ion battery

1. INTRODUCTION

Among the candidates for cathode materials in lithium-based batteries, the olivine-structured $LiFePO_4$, as first proposed by Goodenough and co-workers in 1997 [1], has attracted much interest owing to its significant advantages, including high theoretical capacity (170 mAh g^{-1}), acceptable operating voltage (3.4 V vs. Li^+/Li), environmental benignity, high safety, and low cost [2–7].

However, the main problems with this material are low electronic conductivity and low lithium diffusivity, which prevent its large-scale application in electric vehicles (EVs) and hybrid electric vehicles (HEVs) [8-10]. In order to overcome this drawback, conductive agent coating is used to

enhance the electronic conductivity. Carbon coating is a common method to overcome the limited rate capacity, because the dispersed carbon provides pathways for electron transference, resulting in improvement of the conductivity and electrochemical properties [11-14]. In addition, according to the previous reports, metal oxide dopings [15-19] or NiP alloy [20] are favorable to improving the electrochemical properties of $LiFePO_4$ cathode material. To our knowledge, no publications about MnO_2 doping on the $LiFePO_4$ particle are seen. In this paper, 1-D nano rod structure β-MnO_2 was doped in the $LiFePO_4$ particle by a solid state method. The results demonstrate the electrochemical performance of $LiFePO_4$ cathode material is enhanced by the β-MnO_2 doping.

2. EXPERIMENTAL

Uniform single-crystal nano rod structure β-MnO_2 was synthesized via hydrothermal method: 0.01 mol $MnSO_4$ (A.R. TianJin BODI) and 0.01 mol $(NH_4)_2S_2O_8$ (A.R. TianJin BODI) were dissolved in 60.0 mL deionized water under continuous stirring. The resulting homogeneous solution was then transferred into a Teflon-lined stainless steel autoclave (150.0 mL). The autoclave was sealed and maintained at 140 ℃ for 12 h. Then, the autoclave was allowed to cool to room temperature naturally. Next, the precipitates were centrifuged and then thoroughly washed with water and ethanol, respectively. Finally, the products were dried in vacuum at 60 ℃ overnight for further characterization.

$LiFePO_4$/C was synthesized using $CH_3COOLi{\cdot}2H_2O$ (A.R. TianJin ShenTai Co.), Fe_2O_3 (A.R. TianJin BASF Co.) and $NH_4H_2PO_4$ (A.R. TianJin BODI) as the raw materials in the mole ratio based on the formula of $LiFePO_4$. The starting materials, with added 10 wt.% glucose and a small amount of acetone, were milled by ball-milling at a rotating speed of 350 rpm for 3 h. The influence of the agate milling container and balls can be neglected. Then, the material was decomposed at 350 ℃ for 2 h in a flowing Ar atmosphere. The decomposed products as precursors were pressed into pellets and sintered at 700 ℃ in the same atmosphere for 8 h. To improve the electrochemical properties, as-received nano sized β-MnO_2 powder was used as the doped material, the sample treated with β-MnO_2 doping (as $LiFePO_4$/C/β-MnO_2 composite) was prepared in a procedure similar to the previous one. All reagents are of analytical reagent degree.

The phase structures of the powders were analyzed by X-ray diffraction (XRD) on a DX-2700 diffract meter (DanDong China) with Cu Kα radiation. The powder morphology was observed by a JEOL JSM-5310 scanning electron microscope (SEM).

The electrochemical performance of both pristine $LiFePO_4$/C and β-MnO_2 doped $LiFePO_4$/C were evaluated using coin-type cells (CR2025). A lithium metal foil was used as the anode. Composite cathode films were prepared by mixing of 80 wt.% $LiFePO_4$/C active material, 10 wt.% acetylene black as a conductive additive and 10 wt.% polyvinylidene fluoride (PVDF) as a binder, and N-methyl pyrrolidone (NMP) as a solvent. The paste was then coated onto an aluminum foil, and finally dried under vacuum at 100 ℃ for 10 h before electrochemical evaluation. The electrolyte was a solution of 1 M $LiPF_6$ dissolved in the mixture solution of ethylene carbonate (EC) and dimethyl carbonate (DMC) with volume ratio of 1:1. A micro porous polypropylene sheet (Celgard 2400, Celgard Inc., USA) was used as the separator. The cells were assembled in a dry glove box filled with pure argon.

All the cells were allowed to age for 24 h before testing. The charge-discharge tests were conducted on a battery test system (C2001A, LAND, China) with cut-off voltages of 2.0 V and 4.3 V (versus Li^+/Li) at different current rate at room temperature. The cyclic voltammetry (CV) curves were measured at 0.1 mV s^{-1} within the range of 2.5-4.0 V using Zahner IM6e Electrochemical Workstation (ZAHNER-elektrik GmbH & Co. Germany). To estimate the internal resistance of the coin-cells, the electrochemical impedance spectrum (EIS) was studied by using the same electrochemical workstation, the excitation voltage applied to the cells was 5 mV and the frequency range was between 100 kHz and 10 mHz.

3. RESULTS AND DISCUSSION

3.1 Characterization of the as-synthesized products

The XRD pattern of the β-MnO_2 prepared by the hydrothermal method is shown in Fig. 1.

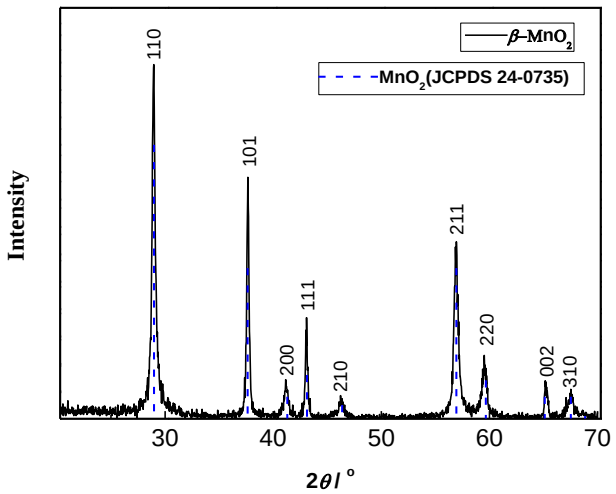

Figure 1. X-ray diffraction patterns of β-MnO_2 obtained by hydrothermal treatment.

All the diffraction peaks can be indexed as tetragonal phase β-MnO_2, which are consistent with the literature (JCPDS 24-0735). SEM image shows that the as-synthesized β-MnO_2 has 1-D nano rod structure with length of 200-400 nm and a diameter of 20-30 nm (Fig. 2a). For brevity, the β-MnO_2 doped $LiFePO_4$/C powder will hereafter be abbreviated as m-LFPO, while the un-doped powder as u-LFPO. Fig. 3 compares the XRD patterns of the u- and m-LFPO powders. The crystalline structure of the $LiFePO_4$/C does not change before and after β-MnO_2 doping process, as shown by the XRD patterns. The well-defined and highly intense peaks demonstrate the presence of olivine $LiFePO_4$ phase. For both patterns, only $LiFePO_4$ and Li_3PO_4 were detected. In general, $LiFePO_4$ samples with

orthorhombic structured Li_3PO_4 were prepared via a carbothermal reduction [21-22]. However, no diffraction lines corresponding to β-MnO_2 phase appeared in the XRD pattern of the m-LFPO.

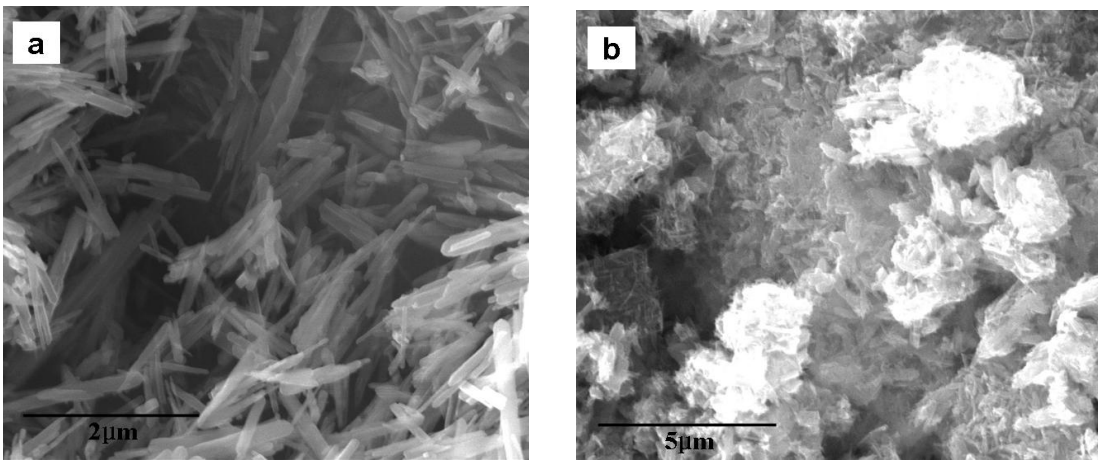

Figure 2. SEM micrograph of (a) β-MnO_2 with 1-D nano rod structure and (b) $LiFePO_4$/C/β-MnO_2.

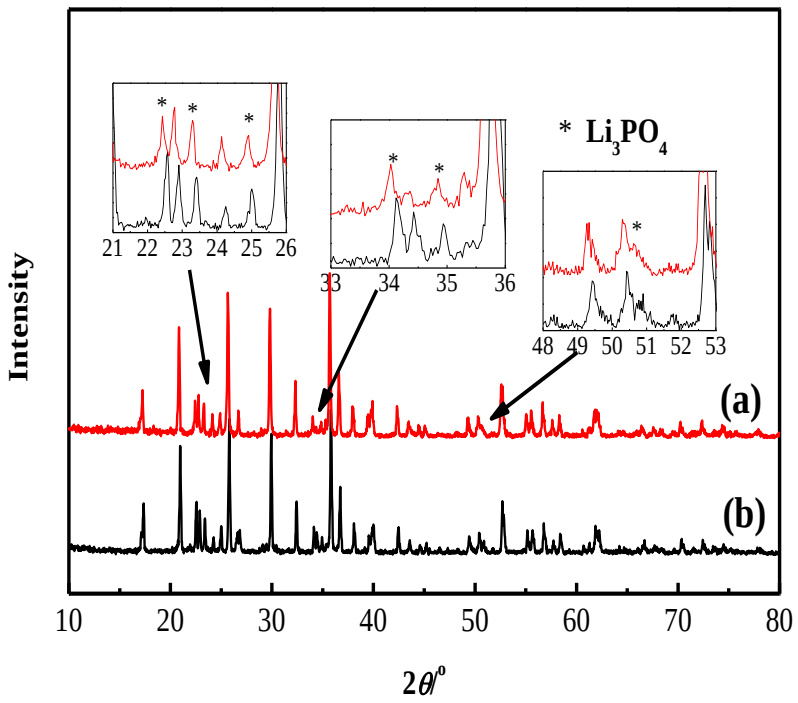

Figure 3. XRD patterns of (a) pristine and (b) β-MnO_2 doped $LiFePO_4$/C.

Indeed, all the strong reflections of the β-MnO_2 phase overlap with the reflections of $LiFePO_4$, and this explains why its presence has not been detected by XRD. The presence of the doping β-MnO_2 was ascertained by the pine needle liked nano rods mixed with $LiFePO_4$/C powders (Fig. 2(b)).

3.2 Electrochemistry characteristics

Cyclic voltammogram (CV) profiles of the m- and u-LFPO, collected at a scanning rate of 1 mV s^{-1}, are shown in Fig. 4. The well-defined reaction peaks of the u-LFPO at 3.765/3.147 V can be attributed to the Fe^{3+}/Fe^{2+} redox couple transformation, accompanied by lithium ion insertion/extraction into and out of the electrode.

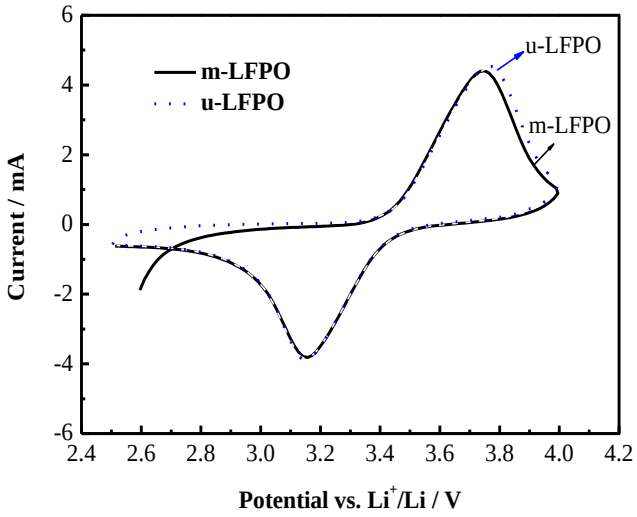

Figure 4. CV profiles of the u- and m-LFPO at the scanning rate 0.1 mV s^{-1}.

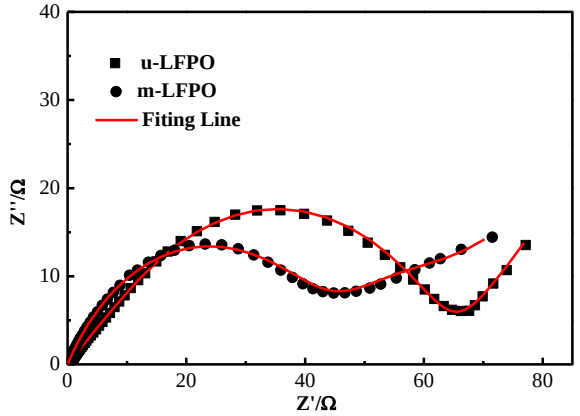

Figure 5. EIS spectra of the u- and m-LFPO electrode in the frequency range between 100 kHz and 10 mHz.

The main Fe^{3+}/Fe^{2+} redox peaks of m-LFPO are located at 3.740/3.155 V. The decrease in the redox potential separation implies that the electrode reactivity is improved by the doping β-MnO_2. Fig. 5 shows the A.C. impedance spectra of the m- and u-LFPO electrodes, which was measured in the fully discharged state after cycling. Impedance spectra of the depressed semicircle represent the

migration of the Li^+ ions at the electrode/electrolyte interface through the solid electrolyte interface layer (high frequency, R_s) and charge transfer process (middle frequency, R_{ct}).

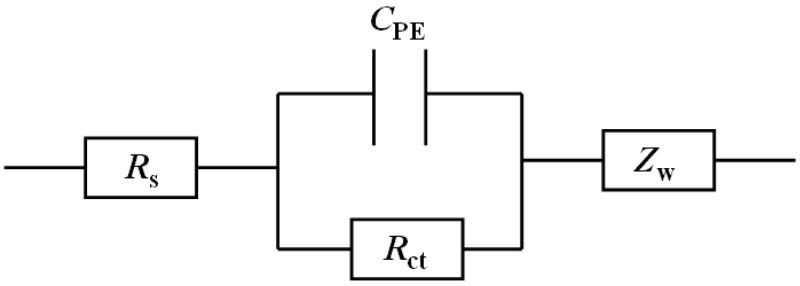

Figure 6. Equivalent circuit used for fitting the EIS experimental data.

Table 1. Electrode kinetic parameters of u- and m-LFPO composite obtained from equivalent circuit fitting of experimental data.

Sample	R_s (Ω)	R_{ct} (Ω)	i_o (mA)
u-LFPO	3.29	65.84	0.390
m-LFPO	4.06	44.85	0.574

i_o, exchange current density of the electrode; $i_o = RT/nFR_{ct}$.

Diffusion of the lithium ions into the bulk of the electrode material represents Warburg impedance (incline line, Z_w). A simplified equivalent circuit model was constructed to analyze the impedance spectra in Fig. 6. The calculated values fit well to the measured values. Parameters obtained from computer simulations using the Zview2.0 software are shown in Table 1. The resistance of the R_s is similar to m- and u-LFPO composites. It is because the cells were prepared by adding the same conductive agent and reaction in the same electrolyte. It was found that the lower charge transfer resistance (R_{ct}) and larger exchange current density (i_o) of the m-LFPO composites, indicating increased charge transfer and reaction kinetics. It is suggested that the improved particle surface due to the doping β-MnO_2 probably is more favorable for lithium ions migration, and therefore enhances the electrochemical performance.

The first charge/discharge profiles of u- and m-LFPO at C/10 are shown in Fig. 7. A flat discharge potential plateau was observed for both the m- and u-LFPO at around 3.4 V, indicating that the two-phase redox reaction proceeds via a first-order transition between $FePO_4$ and $LiFePO_4$ [1]. We noted that the voltage plateau is lengthened for the m-LFPO electrode, which should be attributed to the nano crystals of β-MnO_2 are topotactically active to Li insertion on the first discharge [23]. MnO_2 materials may adopt many polymorphic structures with various MnO_6 octahedral bonding arrangements. This property allows the formation of composites or intergrowths of materials and, as a result, a host of structures may be accommodated. Before the capacity reaches 130 mAh g^{-1}, the discharge curves match with each other perfectly, which indicates that the fundamental nature of the

Li-ion intercalation/de-intercalation $LiFePO_4$ lattices in the early stages of charge/discharge was not affected by the doping.

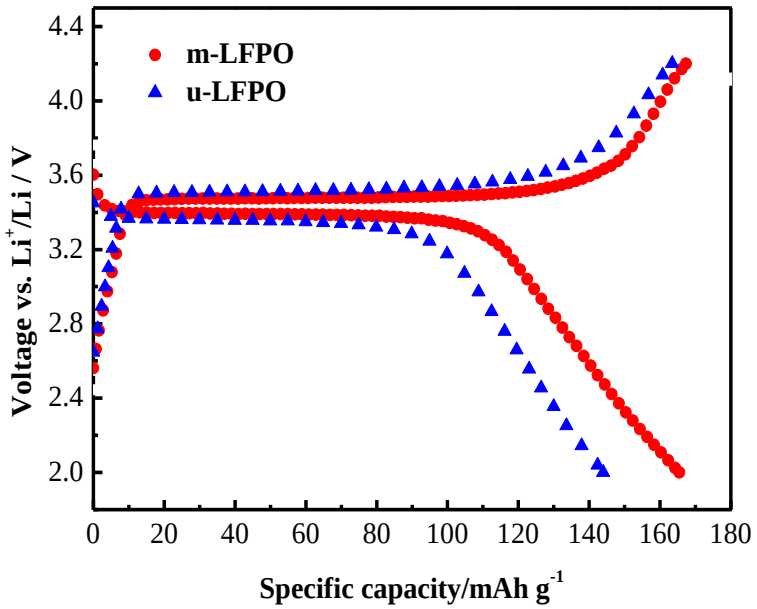

Figure 7. The initial charge/discharge curves of u- and m-LFPO under constant current density of C/10.

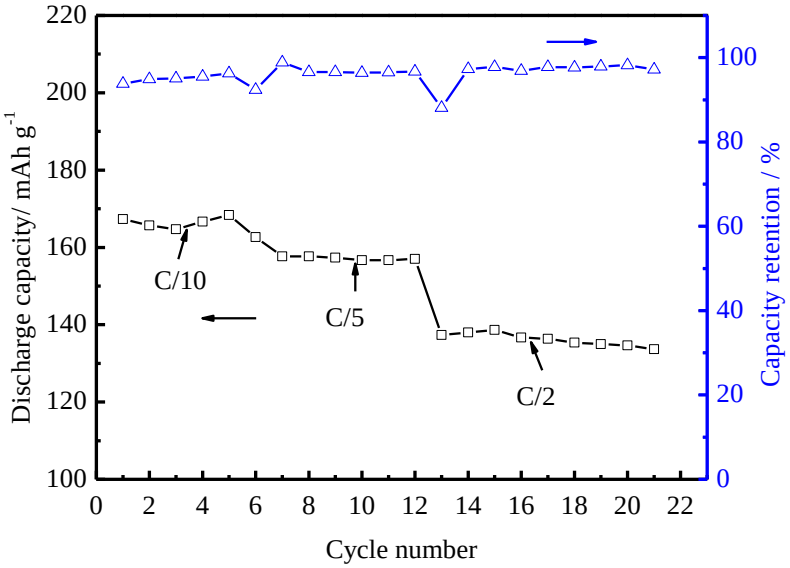

Figure 8. The cycling capability and capacity retention of m-LFPO at various C-rates.

However, after the capacity reaches 130 mAh g^{-1}, the discharge potential of the m-LFPO cell slowly reduces and its discharge capacity could reach higher. The capacity delivery is equal to 167 mAh g^{-1} for charge ($FePO_4$ + Li → $LiFePO_4$) and 165 mAh g^{-1} for discharge ($LiFePO_4$ → $FePO_4$ +

Li). These values are equivalent to an average of 97% of the maximum theoretical capacity, demonstrating exceptionally high conversion of the active material (Fig. 7). In addition, the voltage profiles of m-LFPO show a narrow gap between charge and discharge, indicating very low electrode resistance. The cyclabilities of the m-LFPO at the C/10, C/5 and C/2 rates are shown in Fig. 8. The m-LFPO cell shows a capacity of near 165 mAh g^{-1} at C/10, 158 mAh g^{-1} at C/5 and 140 mAh g^{-1} at C/2. The capacity is between 165-167 mAh g^{-1} at C/10, indicating the activation processes of the cell. The capacity retention is 97.8% after six cycles at C/5 rate and 97.3% after 9 cycles at C/2, respectively. We infer that the 1-D nano rod structure β-MnO_2 doping plays a regulatory role for insertion of the Li-ion into the lattice in later discharge stage, it may have increased the order of lithium ions that occupy the outer lattice sites of the $LiFePO_4$ grains and increase the number of lithium ion into the lattice, thus resulting in voltage drop delay, and capacity increases. This is consistent with the impedance results (Fig. 5).

4. CONCLUSIONS

The $LiFePO_4$/C doped with 1-D nano rod structure β-MnO_2 shows improved electrochemical performance such as higher cycling capacity and lower cell impedance. This is attributed to the presence of β-MnO_2 which effectively prevents the $LiFePO_4$ particles from the direct contact with the electrolyte solution, improving the structural stability, reducing the interfacial resistance and increasing Li-ion conductivity. The β-MnO_2 doping plays a regulatory role for Li-ion inserting the lattice, increasing the order of lithium ion occupied the outer lattice of the particle.

ACKNOWLEDGEMENTS

This work has been supported by the Scientific Research Foundation for the Returned Overseas Chinese Scholars, State Education Ministry (2010-149), Doctoral Researching Fund (HIT(WH)XB200801) and Natural Scientific Research Innovation Foundation in Harbin Institute of Technology (HIT.NSRIF.2011099).

References

1. A.K. Padhi, K. S. Nanjundaswamy, J. B. Goodenough, *J. Electrochem. Soc.* 144 (1997) 1188
2. Y. Zhou, J. Wang, Y. Hu, R. O'Hayre, Z. P. Shao, *Chem. Commun.* 46 (2010) 7151
3. S. W. Oh, S. T. Myung, S-M Oh, K. H. Oh, K. Amine, B. Scrosati, Y-K Sun, *Adv. Mater.* 22 (2010) 4842
4. D. Lepage, C. Michot, G. Liang, M. Gauthier, S. B. Schougaard, *Angew. Chem. Int. Ed.* 50 (2011) 1
5. X. Wu, L. Jiang, F. Cao, Y. Guo, L. Wan, *Adv. Mater.* 21 (2009) 2710
6. M. Zhong, Z. T. Zhou, *Solid State Ionics* 181 (2010) 1607
7. Y.Wang, Y.Wang, E. Hosono, K.Wang, H. Zhou, *Angew. Chem.* 47 (2008) 7461
8. S. B. Petersona, J. Apt, J.F.Whitacre, *J. Power Sources* 195 (2010) 2385
9. F. Y. Kang, J. Ma, B. H. Li, *New Carbon Materials* 26(3) (2011) 161
10. M. Safari, M. Morcrette, A. Teyssot, C. Delacourt, *J. Electrochem. Soc.* 156 (2009) A145

11. J. Chong, S. D. Xun, H. Zheng, X. Y. Song, G. Liu, P. Ridgway, J. Q. Wang, V. S. Battaglia, *J. Power Sources* 196 (2011) 7707
12. K. Zaghib, J. Shim, A. Guerfi, P. Charest, K.A. Striebel, *Electrochem. Solid State Lett.* 8 (2005) A207
13. A.F. Liu, Y. F. Liu, Z. H. Hu, G. Gao, Y. Y. Xu, L. Lei, *J. of Physics and Chemistry of Solids* 72 (2011) 831
14. V. Palomaresa, A. Goni, I. Muro, I. Meatza, M. Bengoechea, I. Cantero, T. Rojo, *J. Power Sources* 195 (2010) 7661
15. H. Liu, G.X. Wang, D. Wexler, J.Z. Wang, H.K. Liu, *Electro. Comm.* 10 (2008) 165
16. Y. D. Li, S. X. Zhao, C. W. Nan, B. H. Li, *J. Alloys and Compounds* 509 (2011) 957
17. H. H. Chang, C. C. Chang, C. Y. Su, H. C. Wu, M. H. Yang, N. L. Wu, *J. Power Sources* 185 (2008) 466
18. J. Yao, F. Wu, X. P. Qiu, N. Li, Y. F. Su, *Electrochimica Acta* 56 (2011) 5587
19. Y. Jin, C.P. Yang, X.H. Rui, T. Cheng, C.H. Chen, *J. Power Sources* 196 (2011) 5623
20. C. S. Li, S. Y. Zhang, F. Y. Cheng, W. Q. Ji, J. Chen, *Nano Res.* 1 (2008) 242
21. Y. Kadoma, J.-M. Kim, K. Abiko, K. Ohtsuki, K. Ui, N. Kumagai, *Electrochim. Acta* 55 (2010) 1034
22. S. H. Wu, J. J. Shiu, J. Y. Lin, *J. Power Sources* 196 (2011) 6676
23. S. J. Christopher, *J. Power Sources* 165 (2007) 559